A Wideband High-Gain Multilinear Polarization Reconfigurable Antenna Integrated With Nonuniform Partially Reflective Surface

Zekui Zhang, Yanhui Liu, *Senior Member, IEEE*, Shu-Lin Chen, Dingzhao Chen, and Yong-Ling Ban

***Abstract*—In this communication, we develop a wideband and high-gain multilinear polarization reconfigurable antenna integrated with nonuniform partially reflective surface (PRS). It leverages a compact L-probe feed source with 25.71° interval reconfigurable LPs. A polarization-independent nonuniform PRS with both reflection magnitude and phase control is introduced to significantly enhance the gain of the feed source. Furthermore, a systematic analysis on antenna gain relative to the PRS size is conducted, and the obtained gain can vary from around 15 to 20 dBi by carefully designing the PRS. Besides, a partial metallic cavity is presented to further improve the peak gain without enlarging the antenna. An example of seven-LP reconfigurable antenna was designed, simulated, and fabricated. The prototype achieves an overlapped −10 dB impedance bandwidth from 9.28 - 11.32 GHz (19.8%) and a maximum gain of 15.08 dBi. The 3-dB gain bandwidth is 15.7% (from 9.4 to 11 GHz). These measured characteristics validate the antenna's good performance in delivering wide bandwidth and high gains across multiple LPs.**

***Index Terms*—High gain, multilinear polarization, nonuniform partially reflective surface (PRS), reconfigurable antennas, wideband.**

I. Introduction

POLARIZATION reconfigurable antennas are recognized for their capacity to suppress fading losses caused by multi-path effects and enhance channel capacity [1]. In many wireless systems, wideband capability and high gain are paramount for ensuring communication range and minimizing signal interference. Thus, several technologies have been reported to meet these performance criteria for polarization reconfigurable antennas. The methods include phased array formation [2], [3], active/passive metasurface utilization [4]–[6] and partially reflective surface (PRS) integration [7]–[15].

For those technologies, phased array antennas based on polarization elements are capable of providing high gain. But they require complex amplitude and phase-control networks. By using active/passive metesurface, usually integrated with a spatial feeding-source, a high gain will achieve for reconfigurable polarizations. For example, the Huygens metasurface transmitarray antenna in [5] obtained a peak gain of 25.89 dBi for the multiple polarizations. However, this spatial feeding approach requires a large focal distance to ensure adequate incidence onto the antenna surface. Recently, PRS antennas have received significant attention due to their simple and compact configurations, and potentially wide bandwidth.

To date, most of the reported polarization reconfigurable antennas integrated with PRS were designed with the polarization switching between a few linear polarizations (LPs), left-handed circular polarization (LHCP) and/or right-handed circular polarization (RHCP). Generally, to facilitate the polarization switching, one can either reconfigure its feed sources [7]–[14] or the PRSs [15]. For example, the antenna reported in [13] achieved a polarization switching among LP, LHCP and RHCP by using a reconfigurable feed source. Yet, this design uses only a uniform PRS, resulting in low aperture efficiency. In addition, while circular polarization (CP) is valuable for receiving arbitrary polarized waves, it can lead to up to 50% power loss, impacting communication range. Therefore, there's growing interest in facilitating multiple LPs with the PRS-integrated polarization reconfigurable antennas. Hence, a uniform PRS integrated two-element slot-coupled patch array was presented in [14]. This antenna achieved two LP states with a −10 dB impedance bandwidth of 21% and a peak gain of 15.1 dBi. In [15], three LP states were obtained by using massive p-i-n diodes on the PRS.

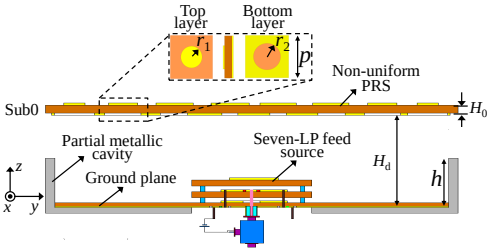

Fig. 1. Geometry of the proposed antenna.

From the above literatures, it is found that realizing multilinear polarization in PRS-integrated antennas while concurrently achieving wideband and high-gain performance, presents several challenges due to the following three aspects. Firstly, none of the reported PRS-integrated polarization reconfigurable antennas can achieve more than four LP states. Secondly, the prevalent reliance on uniform PRS primarily aims at achieving an in-phase electric field, potentially compromising both gain and aperture efficiency. Finally, inherent design difficulties arise when trying to increase the number of LPs, primarily due to the intricate mechanisms associated with reconfigurable feeding microstrip patches and their feed networks. It is worthy to mention that many multilinear polarization reconfigurable patch or dipole antennas have been reported. They are potential candidates for serving as the feed source while integrating with PRS. However, these antennas in [16]–[18] as feed sources usually have narrow impedance bandwidth, low gain or small amount of LPs. For example, polarization reconfigurable antenna in [18] was presented with only four-LPs, utilizing four pairs of bow-tie dipoles. The antenna reported in [19] exhibits a large bandwidth, high gain and larger number of LP states. But it has relatively large electrical size, which will cause impedance mismatching when it is integrated with PRS.

In this communication, a compact wideband polarization reconfigurable feed source is developed and tailored for a seven-LP antenna integrated with a nonuniform PRS. A forming principle of the nonuniform PRS is presented to obtain equal amplitude and in-phase electric field for improving the gain of the feed source while maintaining wideband switchable LPs. For demonstration, a prototype operating at 10 GHz is fabricated and measured. Measurement results show the overlapped −10 dB impedance bandwidth for the seven reconfigurable LPs is from 9.28 GHz to 11.32 GHz. The 3-dB gain bandwidth is 15.7% with a peak gain of 15.08 dBi at 10.6 GHz, and the maximum aperture efficiency is 55.4%. This work is the first to enable a total of seven switchable LPs for PRS-integrated antennas with a compact and easy-integration configuration while maintaining

This work was supported in part by the National Natural Science Foundation of China (NSFC) under Grant U2341208 and in part by the Municipal Government of Quzhou under Grant 2023D010. *(Corresponding author: Yanhui Liu.)*

Z. Zhang, Y. Liu, D. Chen and Y. -L. Ban are with the School of Electronic Science and Engineering, University of Electronic Science and Technology of China, Chengdu 611731, China (e-mail: yhliu@uestc.edu.cn).

S. -L. Chen is with the Global Big Data Technologies Centre (GBDTC), University of Technology Sydney (UTS), Ultimo, NSW 2007, Australia.

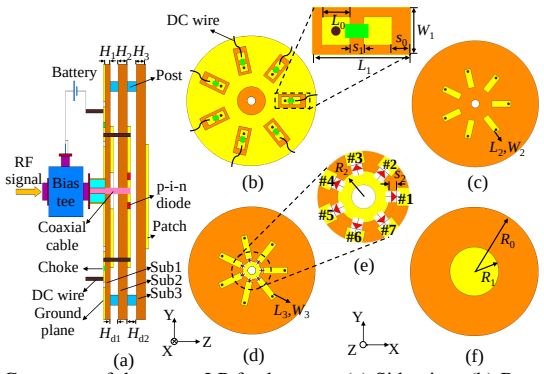

Fig. 2. Geometry of the seven-LP feed source. (a) Side view. (b) Bottom view of Sub1. (c) Top view of Sub1. (d) Top view of Sub2. (e) Partial enlarged top view of Sub2. (f) Top view of Sub3.

wide bandwidth and high gain. Moreover, the antenna gain can be chosen from around 15 to 20 dBi by properly selecting and optimizing the nonuniform PRS. The developed antenna achieves a high figure of merit, making it attractive for many emerging applications.

II. Seven-LP Reconfigurable Antenna Integrated With Nonuniform PRS

A. Antenna Configuration

Fig. 1 shows the cutaway drawing of the developed antenna. This antenna is designed to work at the central frequency of 10 GHz. A seven-LP feed source is centrally located above the ground plane. A polarization independent nonuniform PRS is introduced above the feed source to enhance the gain. The nonuniform PRS consists of two metal layers respectively printed on the bottom and top layers of Sub0. A partial metallic cavity is placed at the bottom to further improve the peak gain and aperture efficiency without enlarging the antenna. Its wall thickness is fixed as 1 mm. Furthermore, a hole with a radius of 10 mm is drilled in the cavity to install the feed source.

Fig. 2 shows the configuration of the seven-LP feed source, which is composed of three substrates: Sub1, Sub2 and Sub3. It's worth noting that for clarity in observation, only a segment of Sub1 is included in Fig. 2(a). These substrates are separated by air gaps with heights of H_{d1} and H_{d2}. The bottom and top views of Sub1 are shown in Fig. 2(b) and (c), respectively. The bottom layer of Sub1 features seven rectangular slots, within which two small pads are printed for DC biasing. An inductor (Green pad) is connected between the two pads to block RF signal. On the top layer of Sub1, seven rectangular patches are printed above the corresponding DC patches, and their dimensions are represented by L_2 and W_2. One function of the rectangular patches is to reduce the associated coupling effect onto the DC biasing pads, and hence to improve the forward radiation. The other function is to expand the operating bandwidth.

Sub2 is a single-layer copper-ladded. A center-fed pad with a radius R_2 and seven rectangular patches with dimensions of L_3 and W_3 are printed on top layer, as shown in Fig. 2(d). The rectangular patch on Sub2 and coaxial line form a L-probe. P-i-n diodes, labeled as #1 - #7, are used to realize the reconfiguration for seven LPs, as shown in Fig. 2(e). In order to ensure symmetry for the seven-LP states, a circular microstrip patch with a radius of R_1 is adopted as the radiating element, as shown in Fig. 2(f). Note that all substrates used in this work are RT/duroid 5880, and its relative permittivity is ε_r = 2.2 and loss tangent tanδ = 0.0009. The key parameter values of the seven-LP feed source are provided in Table I.

B. Design of the Seven-LP Feed Source

Regarding the seven-LP feed source, achieving impedance matching across all states presents a considerable challenge, especially when aiming for a compact design. To address this, we employ seven L-probes that stimulate a single patch. The specific L-probe arm is controlled using p-i-n diodes. Typically, using an L-probe offers an simple yet effective technique to enhance the impedance matching bandwidth of a microstrip patch antenna. Its combination with the radiating patch introduces a capacitance that counteracts some inductance introduced by the probe itself. Furthermore, the radiator of the feed source is compact, with dimensions equivalent to just 0.25λ (λ is the wavelength at 10 GHz in the free space). This allows for its easy integration with PRS. In the design process, it is key that the total length of the L-probe is about λ/4. Also, it has been determined that the height part of L-probe results to the widest bandwidth when it is around 55% of the height between radiation element and ground [20]. For the proposed antenna, the relevant parameters satisfy: H_1+H_{d1}+H_2 = (H_1+H_{d1}+H_2+H_{d2}+H_3)×55%. Typically, the height part of L-probe is chosen to be relatively small, e.g., less than λ/8, to ensure that the length of horizontal part is adequate for optimizing impedance matching. Given the customized heights of the commercial substrates, the selection for H_1 is determined to be 0.5 mm, H_2 as 0.8 mm, and H_3 as 0.8 mm, respectively. Consequently, H_{d1} is chosen as 0.5 mm. Hence, the optimal height of H_{d2} is approximately 0.67 mm. However, for the sake of ease in fixation, we set H_{d2} as a value of 0.5 mm. In addition, the radius R_2 of the center pad on top of Sub2 is selected as a small value 1.1 mm to mitigate interference with different polarizations and to accommodate the soldering of the seven PIN diodes and the inner coaxial probe. Therefore, the length L_3 is around 3.77 mm. Beside, The diameter $2R_1$ of the radiating element is about λ/4.

TABLE I
Key Parameters of the Seven-LP Feed Source

Parameter	H_{d1}	H_{d2}	H_1	H_2	H_3	L_0	L_1	L_2	L_3
Value (mm)	0.5	0.5	0.5	0.8	0.8	1.3	4.0	2.82	3.77
Parameter	W_1	W_2	W_3	S_0	S_1	S_2	R_0	R_1	R_2
Value (mm)	1.9	0.8	0.85	0.5	0.6	0.4	10	3.8	1.1

Taking the conduction of p-i-n diode #1 as an example, Fig. 3(a) shows the surface current distribution on the radiating element. It can be seen that the seven-LP feed source is operated at the TM_{11} mode. This mode helps to achieve good linear polarization performance and directional radiation pattern. The simulated impedance bandwidth in terms of $|S_{11}| \leq -10$ dB is 18.7% (from 9.58 to 11.56 GHz), as shown in Fig. 3(b). Fig. 3(c) displays the radiation patterns at 10 GHz. It can be seen that the proposed seven-LP feed source has good directional radiation characteristics. Fig. 3(d) shows the realized gain and radiation efficiency as functions of the source frequency. Its 3-dB gain bandwidth for realized gain is from 9.45 to 11.82 GHz while the peak gain reaches 6.1 dBi.

For the designed seven-LP feed source, the polarization switching was accomplished by controlling the connection between the center-fed pad and appropriate L-probe arm. Fig. 3(a) shows that the LP state along φ = 0° is obtained when p-i-n diode #1 is ON. Fig. 4 shows the current distributions on the circular microstrip patch when p-i-n diode #3, #5 or #7 is activated ON sequentially. Clearly, each activation corresponds to a unique LP state, with the associated L-probe becoming excited. As a result, the obtained LP states are defined by angles φ = 102.86°, 25.71°, and 128.57°, respectively. For brevity, three additional polarization states along angles 51.43°, 154.29°, and 77.15° are not shown. Notably, the feed source exhibits rotational symmetry for all the LP states.

C. Nonuniform PRS and Gain Analysis

To achieve uniform reflection phase and transmission amplitude, we implemented a nonuniform PRS and further tailored it for compatibility with the seven-LP feed source. Fig. 5 displays the top view

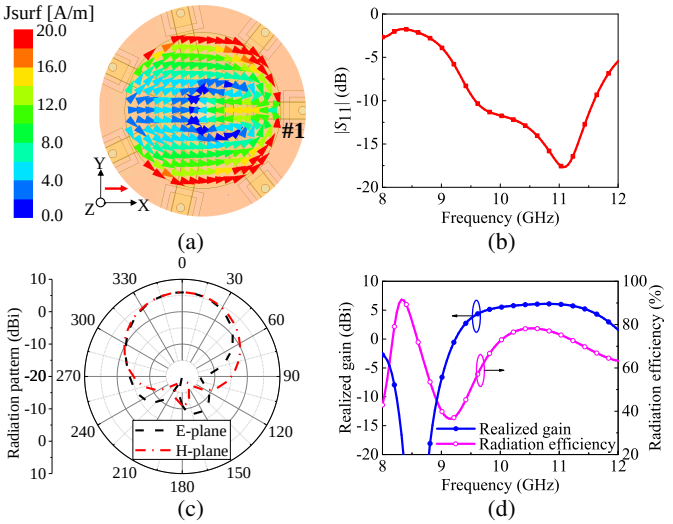

Fig. 3. (a) The surface current distribution. (b) $|S_{11}|$. (c) The radiation patterns at 10 GHz. (d) Realized gain and radiation efficiency.

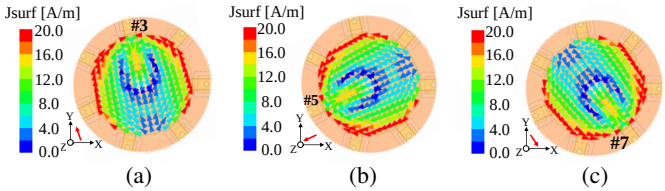

Fig. 4. Simulated current distributions of the seven-LP feed source when different p-i-n diode is ON. (a) #3. (b) #5. (c) #7.

of the proposed nonuniform PRS alongside a simplified ray tracing model. In traditional setups, unit cells of the same color exhibit identical reflection phase and amplitude when incident waves traverse the PRS. Moving from the center to the periphery, the reflection phase for distinct unit cell groups is represented as φ_n (n = 1, 2, 3, 4, ...), and the associated reflection amplitude is denoted by R_n. The symbol E_n signifies the transmitted electric field amplitude. As expounded in [21], peak gain is achieved at $\theta = 0°$. Moreover, the resonance condition and electric field amplitude distribution adhere to the subsequent equations, respectively:

$$H_d = \frac{\lambda}{4\pi}(\varphi_n + \varphi_G + 2m\pi) \quad m = 0, \pm1, \pm2, \cdots \tag{1}$$

$$\begin{cases} E_n = E_0 \cdot \sqrt{1 - R_n^2} & n = 1 \\ E_n = E_0 \cdot \left(\prod_{M=1}^{n-1} R_M \right) \cdot \sqrt{1 - R_n^2} & n = 2, 3, 4 \cdots \end{cases} \tag{2}$$

where φ_G is the reflection phase of ground plane. Usually, m is chosen to be 1, and φ_G is equal to $-\pi$. Therefore, the distance H_d is 15.5 mm (0.5λ at 10 GHz) to satisfy the resonant candition. In addition, when the resonant condition in (1) is satisfied, the aperture electric distribution is in-phase. To achieve the equal amplitude, i.e., E_{n+1} equals to E_n, the reflection magnitude should satisfy:

$$R_n = \sqrt{\frac{1}{2 - R_{n+1}^2}}, \ 0 \le R_{n+1} < 1 \tag{3}$$

Equation (3) implies three important requirements for designing an antenna integrated with nonuniform PRS. 1) The reflection magnitude for unit cell should be decreased from center to edge. 2) Since the reflection magnitude R_{n+1} is equal to 0, the dimension of the substrate for etching the PRS should be large than the size of the nonuniform PRS. 3) The dimensions of the metal ground plane and

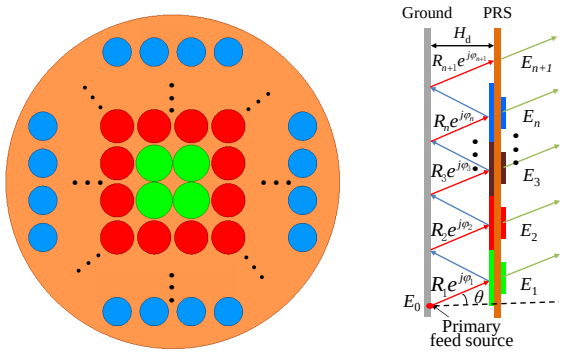

Fig. 5. (a) The top view of the proposed nonuniform PRS, and (b) the simplified ray tracing model.

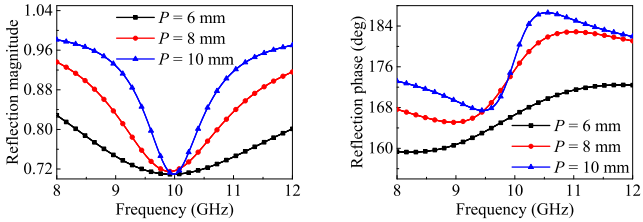

Fig. 6. Reflection (a) phases and (b) magnitudes with different P.

the partial metallic cavity should be at least equal to the size of the substrate for etching the nonuniform PRS, for forcing all the electromagnetic energy radiating via the nonuniform PRS.

Based on the requirements above, the radius R_{Sub0} of Sub0 and the outer radius R_{outer} of the metallic cavity are demonstrated to the same value, equal to nP + 1/2P, where P is the period of unit cell. This choice ensures that the aperture of the proposed antenna is small and also can accommodate all the unit cells. Using n = 4 as a reference, the theoretical reflection magnitudes, transiting from edge to center, are cataloged as: R_4 = 0.71, R_3 = 0.82, R_2 = 0.87, and R_1 = 0.90. Furthermore, it is known that a positive phase slope can enhance the operating bandwidth. For this purpose, we designed a dual-layer PRS based on circular construction as shown in Fig. 1. Moreover, The unit cell's performance is stability against any linearly polarized wave.

In the design process of unit cell, The period P is normally less than λ/2, and a smaller spacing leads to a more stable characteristic versus incidence angle and avoids the onset of sidelobes [22]. To choose an suitable P, we analyze the reflection performances of the unit cell with a period of 6 mm (0.2λ), 8 mm (0.27λ) and 10 mm (0.33λ), respectively. As plotted in Fig. 6(a), the desired reflection magnitude (0.71) can be achieved at 10 GHz for different P. In addition, the reflection phase presents a positive trend around 10 GHz in all these cases, as shown in Fig. (b). Although a large phase difference is more helpful to meet the resonance condition (1), but the band of positive reflection phase decreases as the period P increases from 6 mm to 10 mm. Hence, the period P is selected as 8 mm. And thus the radii of the metal ground plane and the partial metallic cavity are 36 mm. Next, the reflection characteristics for different r_1 and r_2 are analyzed. Fig. 7(a) shows the reflection phases and magnitudes as the radius r_1 increases from 3.58 mm to 3.98 mm. It can be seen that the radius r_1 has an significant influence on the frequency with positive reflection phase, and little effect on the magnitude at the center frequency within the positive reflection phase band. Fig. 7(b) shows the reflection phases and magnitudes as the radius r_2 increases from 2.42 mm to 3.22 mm. Clearly, its effect on the reflection phase and amplitude is opposite to the radius r_1.

Finally, the satisfactory dimensions of the unit cell are obtained by controlling the radii of r_1 and r_2. As noted in Fig. 8(a), the

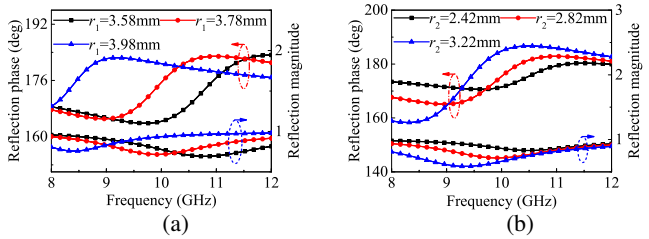

Fig. 7. Reflection (a) phases and (b) magnitudes for r_1 and r_2.

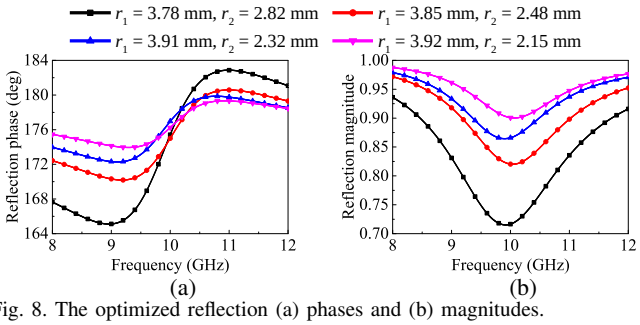

Fig. 8. The optimized reflection (a) phases and (b) magnitudes.

reflection phase demonstrates a positive trend from 9.3 to 10.8 GHz. For different r_1 and r_2 combinations, reflection magnitudes at a central frequency of 10.0 GHz are listed in Fig. 8(b). Compared with the situation of integrating with uniform PRS (r_1 = 3.78 mm and r_2 = 2.82 mm), the gain is improved approximately 1.1 dB at 10 GHz.

Besides the use of nonuniform PRS for gain enhancement, we also introduced a partial metallic cavity to further improve the gain. Fig. 9 shows the electric field distribution within the cavity at 10.0 GHz, during the activation of p-i-n diode #1. As noted in Fig. 9(a), the electric field predominantly occupies the central portion of the cavity in the absence of the partial metallic structure. However, with the integration of the partial metallic cavity, as shown in Fig. 9(b), there is a notable enhancement in the electric field at the periphery of the cavity. This suggests that a larger fraction of electromagnetic energy is radiated via the PRS. The enhanced electric field on PRS also demonstrates that the partial metallic cavity helps to improve forward radiation. Consequently, the realized gain elevates from 13.4 to 15.2 dBi at 10.0 GHz. Importantly, this amplification in gain achieved doesn't increase the antenna aperture.

To generalize the design of our developed high-gain and wideband nonuniform PRS, the cases for different n are explored and analyzed. Within this analysis, the dimensions of the feed source and the height and wall thickness of the partial metallic cavity were kept constant, while the outer radius of the partial metallic cavity is consistent with PRS. The distribution of unit cells to form different apertures was tailored to meet both wideband and high-gain properties. Using the LP state associated with p-i-n diode #1 as a representative example, Fig. 10(a) shows the simulated $|S_{11}|$ when n is increased from 4 to 10. It is noted that the -10 dB bandwidth decreases as increasing n. This is due to the decreased range of positive reflection phase over frequency with the increasing of reflection magnitude. As shown in Fig. 10(b), the gain achieved at 10.0 GHz increases from 15.2 to 20.2 dBi, while the radiation efficiency maintains in the range of 69.8% to 79.8%, when n is increased from 4 to 10. The maximum aperture efficiency reaches 60.5% when n is equal to 5.

D. Parameter Analysis and Design Guideline

To further understand the strategy in obtaining wideband and high gain for the developed multilinear polarization reconfigurable antenna integrated with nonuniform PRS, the key parameters are analyzed. Note that the dimensions of unit cells for forming the nonuniform PRS are fixed and the distance H_d between PRS and

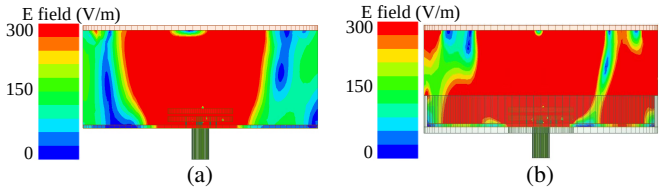

Fig. 9. The electric field in the cavity at 10.0 GHz when p-i-n diode #1 is ON. (a) Unshield cavity. (b) Shield partial metallic cavity.

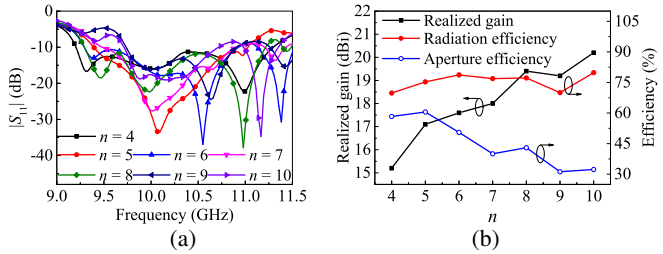

Fig. 10. Simulated results for different n when p-i-n diode #1 is ON. (a) $|S_{11}|$ and (b) realized gain, radiation efficiency and aperture efficiency at 10.0 GHz.

ground is as 15.5 mm. We can infer that the impedance matching characteristics are mainly related to the seven-LP feed source. Fig. 11 shows the impedance matching characteristics for different L_2 and R_2. In addition, the other parameters are kept constant as shown in Table I, and n is set to 4. As shown in Fig. 11(a), the resonant frequency at high frequency decreases from 11.2 GHz to 10.9 GHz as the length L_2 increases from 2.32 mm to 3.32 mm. It leads to a narrower impedance bandwidth. At the low frequency of 9.5 GHz, the reflection coefficient gradually increases. Fig. 11(b) shows the radius R_2 of center-fed pad on impedance matching performance. It is noted that the impedance matching deteriorated near 9.4 GHz and 10.6 GHz, because it is at the key position between the 50 Ω coaxial line and the horizontal part of L-probe. Therefore, an appropriate value R_2 is necessary in the design. And enough space should be considered to weld the p-i-n diodes. Besides, simulated results show that the influence of width W_2 is similar to that of length L_2. And the width W_3 has little effect on the impedance bandwidth. For the proposed antenna, the width W_3 should be as small as possible so that multiple L-probes can be arranged. Finally, we conduct the investigation for the cavity height h and the simulated results are shown in Fig. 12. From Fig. 12(a), it can be seen that the height h has little effect on the impedance matching characteristics. However, it has effect on the obtained gain as shown in Fig. 12(b). When the height h is equal to 5 mm, a maximum realized gain of 15.2 dBi is reached. It is worth noting that the height of the metallic cavity is not fixed for developing such a system at different frequency.

To provide a general guideline for the developing antenna, the design methodology is summarized as follows:

1) Designing a wideband feed source capable of supporting seven LPs: The total length of the vertical part (H_1 + H_{d1} + H_2) and horizontal part (R_2 + S_2 + L_3) for the L-probe is about λ_0/4 (λ_0 is the wavelength at the expected frequency in the free space). And the length of the vertical part is at approximately 55% of the distance between the radiating element and the ground. The diameter of the radiating element is λ_0/4.

2) Developing a wideband PRS element characterized by a positive reflection phase: A smaller period P is reasonable (normally less than λ_0/2), but with the range of positive reflection phase taken into consideration. The radii of the upper circular patch and the bottom circular slot are optimized to obtain the satisfactory reflection phases and magnitudes. Generally, we can increase the radius r_1 from a small value to make the slope of the reflection phase over required frequency positive. And then increase the radius r_2 from a small value to obtain a satisfactory reflection magnitude.

TABLE II
PERFORMANCE COMPARISON OF POLARIZATION RECONFIGURABLE ANTENNAS INTEGRATED PRS

Ref.		No. of states		Overlapped BW (%)	Peak gain (dBi)	3-dB gain BW* (%)	Aperture size (λ_0^2)	Max. aperture efficiency (%)	Profile (λ_0^{**})
		LP	CP						
[10]		1	2	4.0	15.1	-	4.00	42.3	0.6
[11]		1	2	13.1	11.2	8	3.35	31.3	1.19
[12]		2	2	20	9.87	19.6	1.30	45.7	0.067
[13]		3	2	12	14.1	11.4	2.8	24.8	0.61
[14]		2	0	21	15.1	14.6	6.15	41.9	0.50
[15]		3	0	-	15.4	-	11.11	24.8	0.53
This work	n = 4 (Mea.)	7	0	19.8	15.08	15.7	4.52	55.4	0.58
	n = 7 (Sim.)	7	0	13.7	18.0	10.1	12.98	40.0	0.58
	n = 10 (Sim.)	7	0	10.0	20.2	9.1	26.41	32.3	0.58

BW^* is the abbreviation for bandwidth. λ_0^{**} is the wavelength at the center frequency of corresponding reference.

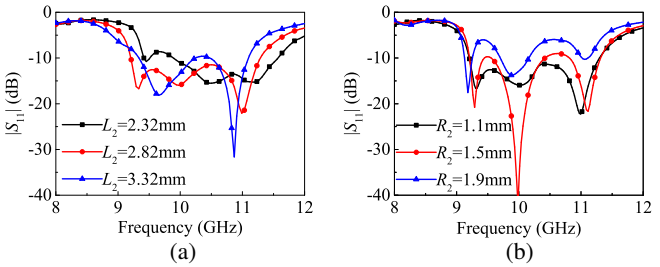

Fig. 11. The simulated $|S_{11}|$ for different (a) L_2 and (b) R_2.

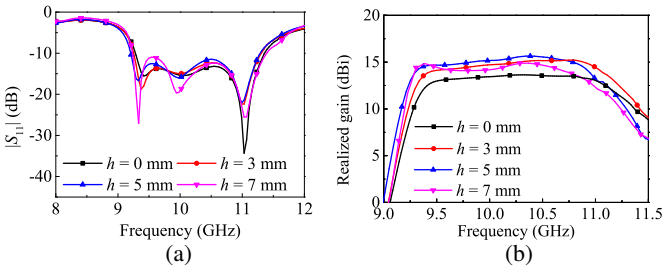

Fig. 12. The simulated (a) $|S_{11}|$ and (b) gain for different h.

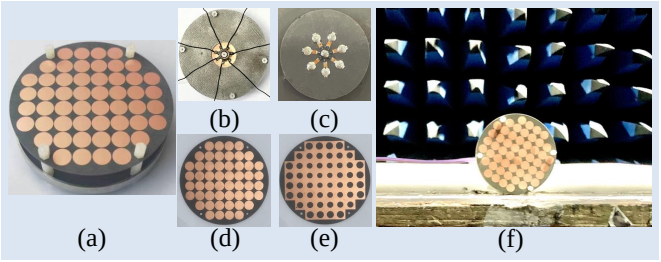

Fig. 13. (a) Overall structure. (b) Bottom view of Sub1, (c) Top view of Sub2. (d) Top view of PRS. (e) Bottom view of PRS. (f) Measurement setup.

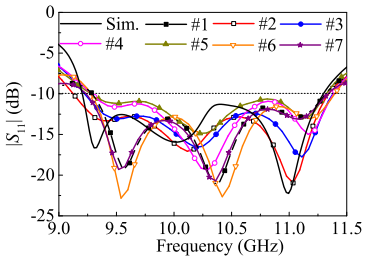

Fig. 14. The simulated and measured $|S_{11}|$.

3) Implementing a nonuniform PRS with properly distributed elements: Based on the expected gain, the scale of the PRS is determined. To allow all electromagnetic energy to radiate into free space through PRS, the radius R_{sub0} of substrate supporting the PRS needs to be set to nP + 1/2P (n = 1, 2, 3, 4, ...). Also, the radius of metallic cavity is equal to R_{sub0}. The height of metallic cavity should be carefully selected to achieve a high gain.

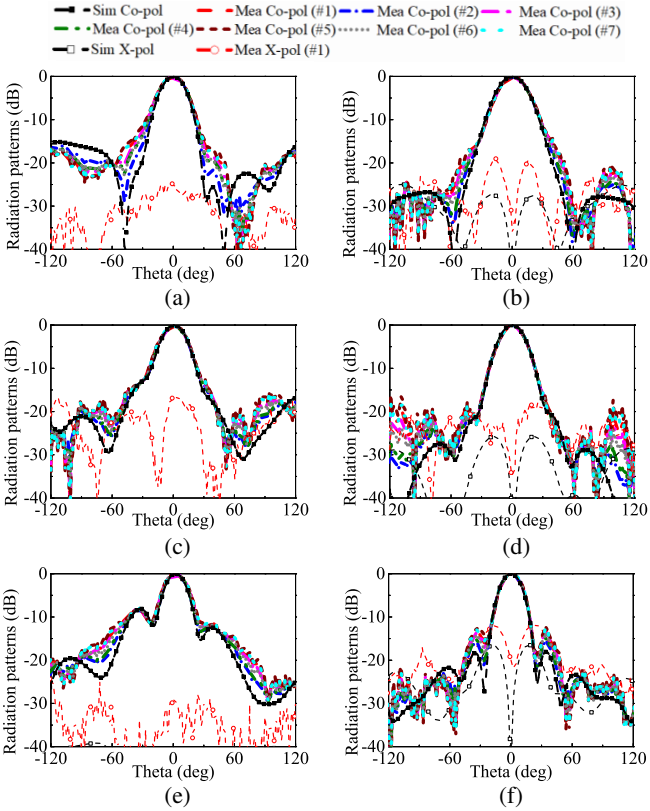

Fig. 15. Simulated and measured radiation patterns of the proposed antenna. (a) E-plane at 9.4 GHz. (b) H-plane at 9.4 GHz. (c) E-plane at 10.0 GHz. (d) H-plane at 10.0 GHz. (e) E-plane at 10.6 GHz. (f) H-plane at 10.6 GHz.

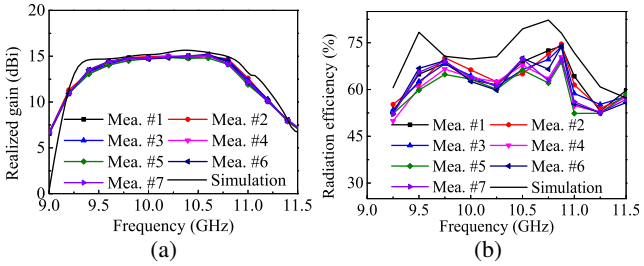

Fig. 16. Simulated and measured (a) gains and (b) radiation efficiencies versus frequency.

III. FABRICATION AND MEASURMENTS

In order to validate the aforementioned antenna performance, we fabricated and measured a prototype of multilinear polarization reconfigurable antenna integrated with nonuniform PRS while n = 4 (four different dimensions of unit cells). The M/ACOM p-i-n diode, MA4AGFCP910 is used in this work. This diode is simulated as a RL circuit with R = 5.2 Ω, L = 30 pH for ON state, and a lumped capacitance of C = 18 fF for OFF state. The DC biasing wires are isolated from RF signals by 3.2 nH inductors from MURATA, model

LQW15AN3N2B00D. Fig. 13 shows the photos of the fabricated multilinear polarization reconfigurable antenna and measurement setup in a microwave chamber. Fig. 14 shows the simulated and measured $|S_{11}|$ when p-i-n diode #1 - #7 is sequentially switched ON respectively. The antenna was measured using a far-field antenna measurement system in a microwave chamber. For all the seven-LP states, the measured overlapped -10 dB bandwidth is from 9.28 to 11.32 GHz, while the simulated one is from 9.19 to 11.20 GHz. The difference is due to possible fabrication inaccuracies.

Fig. 15 shows the simulated and measured radiation patterns in both E- and H-planes at 9.4, 10.0 and 10.6 GHz, respectively. During measurements, one challenge arises from using a single battery for biasing to minimize costs. This adjustment for measuring all polarization states may cause slight variations in the radiation patterns, particularly in the sidelobe region, leading to minor inconsistencies in the reproducibility of the results. This issue can be mitigated by using a multi-channel power supply. However, it will increase the complexity and cost. In addition, the simulated cross polarization curves at E-planes are not displayed in Fig. 15, due to their low level. Also, due to symmetrical configuration, the cross-polarizations at H-planes are presented only when p-i-n diode #1 is ON. As shown in Fig. 15, the measured results for each LP state agree well with the simulated ones, and the cross-polarization level is lower than -18 dB within the main beams at different frequencies. The simulated and measured radiation gains, and efficiencies calculated based on the measured gains are shown in Fig. 16. The developed multilinear polarization reconfigurable antenna achieves 3-dB gain bandwidth of 15.7% with peak gain of 15.08 dBi at 10.6 GHz. The measured gain is lower than the simulated one, which is mainly caused by the lossy bias tee and the influence of RF blocking devices. The measured radiation efficiency is ranging from 48.4% to 74.6% in the band of 9.28 GHz to 11.32 GHz. In addition, the measured gain is about 14.95 dBi at 10.0 GHz, and it is 9.42 dBi higher than of the seven-LP feed source. The maximum aperture efficiency is 55.4% at 9.8 GHz.

To evaluate the performance of our developed multilinear polarization reconfigurable antenna, we compared its performance against recent endeavors in polarization reconfigurability integrated with PRS, as summarized in Table II. Compared with Ref. [14], our antenna achieves a comparable wide band and high gain with smaller electric size by integrating with nonuniform PRS. Moreover, our antenna achieves much more LP reconfigurable states. In fact, out antenna has the highest number of LP reconfigurable states among those PRS-integrated antennas. In addition, the aperture efficiency of our work is obviously higher than those in [10]–[15]. Overall, our developed antenna achieves a large number of reconfigurable LPs while maintaining a wide band, high gain and high aperture efficiency.

IV. Conclusion

In this communication, a wideband and high-gain seven-LP reconfigurable antenna integrated with a nonuniform PRS was developed and fabricated. The wideband and high-gain characteristics were achieved by appropriately modulating the amplitude and phase on the nonuniform PRS. The polarization switching was conveniently accomplished by controlling the connection between the center-fed pad and appropriate L-probe arm using p-i-n diodes on the feed source. The finalized multilinear polarization reconfigurable antenna has successfully obtained a peak gain of 15.08 dBi with a bandwidth of 19.8% and a maximum aperture efficiency of 55.4%, showing significant improvement compared to relevant literatures on polarization reconfigurable antennas integrated with PRS. As with a high figure-of-merit, i.e., having various LP directions, being wide band, and having relatively high gain, the developed antenna has significant application for radars and other emerging systems.

References

[1] C. G. Christodoulou, Y. Tawk, S. A. Lane, and S. R. Erwin, "Reconfigurable antennas for wireless and space applications," *Proc. IEEE*, vol. 100, no. 7, pp. 2250-2261, Jul. 2012.

[2] D. Chen *et al*., "A polarization programmable antenna array," *Engineering,* vol. 16, no. 9, pp. 110-114, Sep. 2022.

[3] Z. X. Wang *et al*., "A planar 4-bit reconfigurable antenna array based on the design philosophy of information metasurfaces," *Engineering,* vol. 17, pp. 64-74, Jul. 2022.

[4] W. Liu, J. C. Ke, C. Xiao, L. Zhang, Q. Cheng, and T. J. Cui, "Broadband polarization-reconfigurable converter using active metasurfaces," *IEEE Trans. Antennas Propag.,* vol. 71, no. 4, pp. 3725-3730, Apr. 2023.

[5] C. Bian, D. Zhou, Y. Zhang, D. Lv, H. Deng, and D. Zhang, "A multipolarization folded transmitarray antenna based on Huygens metasurface," *IEEE Antennas Wireless Propag. Lett.,* vol. 22, no. 12, pp. 2783-2787, Dec. 2023.

[6] K. Li, T. Zhou, Y. Cai, S. Liu, F. Wang, and Y. Ren, "A reconfigurable beam-scanning reflectarray with switchable polarization using independently controlled dual-linearly polarized units," *IEEE Antennas Wireless Propag. Lett.,* vol. 23, no. 5, pp. 1508-1512, May 2024.

[7] C. Ni, C. Liu, Z. Zhang, M. Chen, and X. Wu, "Design of broadband high gain polarization reconfigurable Fabry-Perot vavity antenna using metasurface," *Frontiers Phys.,* vol. 8, pp. 1-9, Aug. 2020.

[8] H. L. Zhu, S. W. Cheung, X. H. Liu, and T. I. Yuk, "Design of polarization reconfigurable antenna using metasurface," *IEEE Trans. Antennas Propag.,* vol. 62, no. 6, pp. 2891-2898, Jun. 2014.

[9] C. Ni, M. S. Chen, Z. X. Zhang, and X. L. Wu, "Design of frequency-and polarization-reconfigurable antenna based on the polarization conversion metasurface," *IEEE Antennas Wireless Propag. Lett.,* vol. 17, no. 1, pp. 78-81, Nov. 2018.

[10] H. H. Tran and H. C. Park, "A simple design of polarization reconfigurable Fabry-Perot resonator antenna," *IEEE Access,* vol. 8, pp. 91837-91842, May 2020.

[11] L. -Y. Ji, P. -Y. Qin, Y. J. Guo, C. Ding, G. Fu, and S. -X. Gong, "A wideband polarization recongurable antenna with partially reflective surface," *IEEE Trans. Antennas Propag.,* vol. 64, no. 10, pp. 4534-4538, Oct. 2016.

[12] J. Hu, G. Q. Luo, and Z. -C. Hao, "A wideband quad-polarization reconfigurable metasurface antenna," *IEEE Access,* vol. 6, pp. 2169-3536, Oct. 2017.

[13] P. Yang, B. Dang, L. Li, Z. Ren, R. Dang, and H. Jia, "Multi-polarized Fabry-Pérot resonator cavity using multilayer partially reflective metasurface in X-band," *J. Phys. D Appl. Phys.,* vol. 144, no. 3, pp. 30001, Nov. 2023.

[14] R. Lian, Z. Tang, and Y. Yin, "Design of a broadband polarization-reconfigurable Fabry-Perot resonator antenna," *IEEE Antennas Wireless Propag. Lett.,* vol. 17, no. 1, pp. 122-125, Jan. 2018.

[15] Y. -G. Jeon, G. R. Yun, J. Kim, and D. Kim, "Polarization reconfigurable high-gain Fabry-Perot cavity antenna," *IEEE Trans. Antennas Propag.,* vol. 70, no. 9, pp. 7727-7734, Sep. 2022.

[16] W. Lin and H. Wong, "Multipolarization-reconfigurable circular patch antenna with L-shaped probes," *IEEE Antennas Wireless Propag. Lett.,* vol. 16, pp. 1549-1552, Jan. 2017.

[17] H. H. Tran, N. N. Trong, T. T. Le, A. M. Abbosh, and H. C. Park, "Low-profile wideband high-gain reconfigurable antenna with quad-polarization diversity," *IEEE Trans. Antennas Propag.,* vol. 66, no. 7, pp. 3741-3746, Jul. 2018.

[18] K. Yang, N. Kou, and S. Yu, "Wideband multi-linear polarization reconfigurable antenna for wireless communication system," *Prog. Electromagn. Res. Lett.,* vol. 117, pp. 75-81, Feb. 2024.

[19] D. Chen, Y. Liu, S. -L. Chen, P. -Y. Qin, and Y. J. Guo, "A wideband high-gain multilinear polarization reconfigurable antenna," *IEEE Trans. Antennas Propag.,* vol. 69, no. 7, pp. 4136-4141, Jul. 2021.

[20] A. G. Koutinos, D. E. Anagnostou, R. Joshi, S. K. Podilchak, G. A. Kyriacou, and M. T. Chryssomallis, "Modified easy to fabricate E-shaped compact patch antenna with wideband and multiband functionality," *IET Microw. Antennas Propag.,* vol. 12, no. 3, pp. 326-331, Jan. 2018.

[21] Q. Chen, Q. Wang, X. Huang, and X. Chen, "A novel method for high-gain and high-aperture efficiency Fabry-Perot resonator antenna design," *Int. J. RF Microw. Comput. Aided Eng.,* vol. 32, no. 6, pp. e23154, Feb. 2022.

[22] B. A. Munk, "Frequency selective surfaces," in *Theory and Design.* New York, NY, USA: Wiley, 2000, pp. 26-52.